Materials Chemistry and Physics 240 (2020) 122222

Contents lists available at ScienceDirect

Materials Chemistry and Physics

journal homepage: www.elsevier.com/locate/matchemphys

Pressure-induced amorphization, mechanical and electronic properties of zeolitic imidazolate framework (ZIF-8)

Mustafa Erkartal [a,*], Murat Durandurdu [a,**]

[a] Abdullah Gül University, Materials Science & Nanotechnology Engineering, Kayseri, Turkey

HIGHLIGHTS

- Pressure induced transitions of ZIF-8 in a wide pressure-range was investigated by using ab initio simulations.
- Crystalline-crystalline and crystalline-amorphous phase transitions were observed.
- Mechanical and electronic properties were accurately estimated.
- The compression and tension strengths of the framework were found significantly different, as in compact bones.

GRAPHICAL ABSTRACT

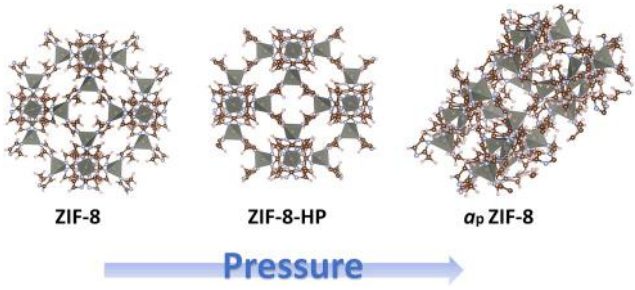

ARTICLE INFO

Keywords:
Metal-organic frameworks
First principle calculations
Pressure-induced amorphization
Amorphous ZIFs

ABSTRACT

Ab initio molecular dynamics (AIMD) simulations are carried out to probe the high-pressure behavior of ZIF-8 over wide pressure-range. Under compression, the enormous distortions in the ZnN_4 tetrahedral units lead to a crystal-to-amorphous phase transition at around 3 GPa. During the amorphization process, the Zn-N coordination is retained. No other phase change but a possible fracture of the system is proposed above 10 GPa. Depending on released pressures, amorphous states with different densities are recovered. Yet when the applied pressure is released just before the amorphization, the rotations of imidazolate linkers (swing effect) cause an isostructural crystal-to-crystal phase transition, in agreement with experiments. In the tensile regime, no phase transition is perceived up to −2.75 GPa at which point the structural failure is observed. The crystal-amorphous phase transitions are also discovered at around 4 GPa under uniaxial compressions. The amorphous structures formed under uniaxial stress are about 20% denser than the one formed under the hydrostatic pressure. The average Young's modulus and Poisson's ratio of ZIF-8 are estimated to be around 5.6 GPa and 0.4, respectively. Interestingly, the tensile strength of ZIF-8 is found to be about 50% greater than its compressive strength. This paper shows that the experimentally observed phase transitions can be successfully reproduced with a clear explanation about the transition mechanism(s) at the atomistic level and all mechanical properties can be accurately calculated for a given ZIF structure by using AIMD simulations.

* Corresponding author.
** Corresponding author.
E-mail addresses: merkartal@mail.com (M. Erkartal), murat.durandurdu@agu.edu.tr (M. Durandurdu).

https://doi.org/10.1016/j.matchemphys.2019.122222
Received 1 July 2019; Received in revised form 28 August 2019; Accepted 23 September 2019
Available online 25 September 2019

1. Introduction

Pressure-induced amorphization (PIA), a transition between crystal and amorphous phases, is attracting a widespread of interest due to its importance in materials science, physics and chemistry [1,2]. It is also considered as an alternative method to produce novel amorphous solids that may be structurally different from those fabricated by the commonly used methods, i.e. the rapid quenching of the melts [2]. The PIA phenomenon was first observed in ice (H_2O) [3], and shortly afterwards discovered in quartz [4] and coesite forms of SiO_2 [5]. The existence of PIA in various types of materials [2] has been demonstrated in later studies. So far, several suggestions have been proposed to explain the underlying mechanisms of PIA, including the breakdown of Born stability conditions [6], kinetic hindrance of phase transitions to a thermodynamically stable high-pressure phase [7], poly-tetrahedral packing [8] and so on [1]. However, there is no generally accepted picture on the driving force(s) of such a solid-state amorphization.

Zeolitic imidazolate frameworks (ZIFs), a sub-class of metal-organic frameworks (MOFs), are currently attracting considerable interest by reason of their relatively high chemical and thermal properties [9]. They also offer promising potentials for gas storage [10–13], catalysis [14–16] and electrochemical [17–19] applications. They possess zeolite topologies, wherein each tetrahedral metal nodes (M = Zn(II) or Co(II)) coordinates to imidazolate-based linkers ($Im^- = C_3H_3N_2^-$) to form (M $(Im)_2$) neutral open framework structure [12,20]. Specifically, the M-Im-M coordination linkage in ZIFs subtends an angle of around 145° at Im ring center, equivalent to the Si-O-Al angle in aluminosilicate zeolites [12,21]. ZIF-8 ($C_8H_{10}N_4Zn$), zinc tetrahedral bridged 2-methylimidazolate (mim), has a high symmetry sodalite (SOD) topology and crystallizes in the cubic I43 m space group (a = 16.992 Å) [21]. The pores with a diameter around 12 Å connected by 3.5 Å diameter six-ring apertures with the 4-ring yield a large pore volume, ~2400 $Å^3$ [22].

Pressure-induced transition (PIT) investigations on MOFs are generally categorized into two groups in the literature: adsorption-induced transitions (AIP), and mechanical-stress induced transitions (MSIT) [23,24]. AIP studies have mainly focused on clarifying the relationship between structural distortions and adsorbent (framework) –adsorbate (e.g. N_2) interactions during the adsorption process [25–28]. The common technique for monitoring phase transitions in the MOFs is the diamond anvil cell (DAC) experiment, in which the frameworks are exposed to a hydrostatic pressure by means of pressure-transmitting medium (PTM) [22,29]. However, because of the pores being filled with PTM molecules, the framework changes to a more resilient structure, which causes a delay in amorphization pressure [30]. In addition, the results may be controversial due to framework-PTM molecules interactions and changes in the physical properties of the carrier fluid under high pressure [31]. So far, in situ TEM compression method was proposed to investigate the direct amorphization process of a single crystal MOF and its mechanical properties [31]. However, it is improbable that these experiments are widely available for now because of the equipment infrastructure required.

As a promising engineering material family, it is vital to determinate the mechanical properties and critical transitions pressure/temperature of the MOFs. A key problem with much of literature on determination of them for MOFs is use of gas molecules or liquids as PTM in both experimental and computational studies. Although these reports provide crucial information for some applications (such as gas adsorption, separation), it is not possible to reveal the mechanical properties of the frameworks reliably by using this method. Since the aforementioned experimental methods are not widely available for now, the most appropriate method is computational material tools. To date, the mechanical properties of ZIF-8 have been studied with both classical molecular dynamics (MD) and density functional theory (DFT) simulations. But as far as we know, such a wide pressure range has never been studied before. So in this work, we reported the high-pressure behavior of desolvated ZIF-8 over a wide compression and tension stresses ranging from −2.75 GPa to 50 GPa using ab initio molecular dynamics (AIMD) simulations, inspired by Suslick's [31] in-situ TEM compression study and Hu's [30] DAC experiment. We witnessed a crystal-amorphous phase transition, a possible fracture of the material on compression, and a crystal-crystal phase change upon decompression through the simulations. The amorphization took place under uniaxial compression as well. Under tension, the framework was failed at −2.75 GPa. The mechanical and electronic properties of the framework were also investigated.

2. Methodology

The optimization of the structure and the behavior of ZIF-8 as a function of pressure were studied by a LCAO (Linear Combination of Atomic Orbitals)-based DFT approach as implemented in the SIESTA (version 3.2) code [32]. The Perdew-Burke-Ernzerhof (PBE) generalized gradient approximation (GGA) [33] for the exchange-correlation potentials and non-local norm conserving Troulier-Martins pseudopotentials [34] were used to define the ion-electron interactions. The Kohn-Sham orbitals were expanded by numerical orbital basis sets with double-ζ polarized (DZP) functions. Real space integration was performed on an ordered grid corresponding to a plane-wave cut off of 250 Ry and only Γ-point sampling of k-mesh was used. All calculations were performed with periodic boundary conditions.

Starting coordinates and lattice parameters were taken from X-ray diffraction derived structure of ZIF-8 [20]. The geometry optimization was performed by a conjugate gradient (CG) variable cell method based on the independent variation of both atomic positions and unit cell parameters. Once the force tolerance criterion of 0.001 eV/Å was achieved, the structure was considered to be optimized. Pressure studies were performed based on the Parrinello-Rahman method [35] with the power quench technique under isoenthalpic-isobaric (NPH) ensemble. A period of 5000 MD steps was applied to have equilibrium state at each pressure step. Also, additional 5000 MD steps were run at and before the phase transitions to guarantee that the system reached to the true equilibrium volume. The time step for each MD simulation was 1 fs (fs). Pressure was applied to the framework as follows: The optimized zero-kelvin structure was used as starting geometry and pressure (P) was increased (or decreased) with a ΔP pressure step. At each new pressure P+ ΔP, the pressure was applied to the structure obtained from the previous pressure (P). The ΔP was 0.25 GPa from −2.75 to 5 GPa, 1 GPa from 5 GPa to 10 GPa, and 2 GPa from 10 GPa to 50 GPa. Thence, we were able to simulate the pressure dependence of the framework and explore the first/second order phase transitions. Through the study, two different types of pressure were applied to the structure. Under hydrostatic pressure, the simulation box was compressed or tensioned in all three directions. To apply uniaxial pressure, we compressed or tensioned the simulation box along the [100] for x, [010] for y and [001] for z directions. A dispersion correction term was not used through the calculations since the framework materials were less influenced by van der Waal-type interactions [36]. The VESTA [37] program for visualization of the obtained structures and the ISAACS code [38] for further structural analysis were used. Optimized computational coordinates of ZIF-8 and a_pZIF-8 have been included in the SI as.xyz files.

3. Results & discussion

3.1. Structural properties and pressure-induced amorphization

The cell parameter ($a = 17.01$ Å) and bulk modulus ($K = 8.46$ GPa) of the relaxed ZIF-8 structure provided in Table 1 are in excellent agreement with the experimental data [39], emphasizing the validity of our simulation. Fig. 1 presents the hydrostatic pressure dependence of the unit cell volume. The volume shows a gradual decrease of approximately 22% up to 2.5 GPa. Then, the volume drastically reduced at 3.0 GPa, indicating a first order phase transition. Beyond this pressure, the framework less reacts to the applied pressure, and the change in the

Table 1
Mechanical properties of ZIF-8.

Constant/ Unit	This work (GGA-PBE (0 K)	Ortiz et al. (MD) [47]	Tan et al. [39] Exp. (Brilloun Scattering (295K)	Tan et al. [39] PBE (0 K)
a (Å)	17.01	–		17.26
C11 (GPa)	10.02	11.3	9.52	10.14
C12 (GPa)	7.69	7.6	6.87	8.00
C44 (GPa)	1.22	2.7	0.97	0.78
K (GPa)	8.46		7.75	8.71
GV (GPa)	1.198		1.11	0.90
GR (GPa)	1.197		1.08	0.87
GH (GPa)	1.1975		1.095	0.885
E (GPa)	3.43		3.145	2.57
ν	0.43		0.43	0.45
vt (m/s)	1140			~1200
vl (m/s)	3258			~3100
vm (m/s)	1296			

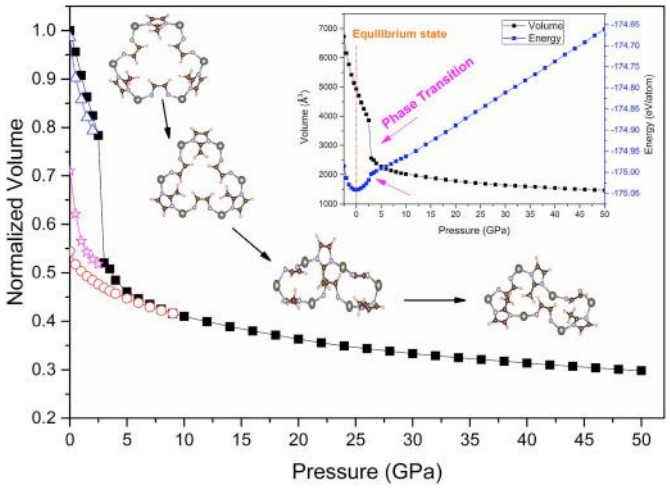

Fig. 1. The hydrostatic pressure dependence of ZIF-8 unit cell. Solid data represents an increase in pressure. The blue, pink and red open data show releasing of pressure from 2.5, 3 and 10 GPa respectively. (For interpretation of the references to colour in this figure legend, the reader is referred to the Web version of this article.)

volume is around 15% in the pressure range of 3.5–50 GPa. Fig. 2a shows total pair distribution functions (PDF) of ZIF-8 as a function of pressure. Until the transition occurs, the structure preserves its symmetry because the PDFs for 0 and 2.5 GPa structures remain almost the same. On the other hand, beyond the short-range order (SRO) defined as the distance between two Zn^{2+} (6 Å), there is no significant peak belonging to ZIF-8 at 3 GPa, indicating that framework does not have a long-range order, namely it is amorphous. At 10 GPa and higher pressures, $g_{Zn\text{-}Zn}(r)$ (6 Å), $g_{Zn\text{-}N}(r)$,(4.2 Å) eventually diminish. However, the pattern below 3 Å is the same for all pressure ranges, providing evidence for the preservation of integrity of the imidazole rings (Figs. S2–S6).

According to the coordination number (CN) analysis performed using the ISAACS code, no coordination modification is observed during the pressure-induced amorphization and the CN of Zn is 4. At 10 GPa, it drops to 3.67, i.e., some Zn-N bonds are broken in this pressure. The CN of Zn decreases gradually to 2.54 at 30 GPa. Beyond this pressure, CN of Zn firstly drops to 2 at 40 GPa and then, to 1.6 at 50 GPa (Fig. 2c). Our critical pressure for the hydrostatic compression correlates fairly well with the experimental amorphization pressure of 4 GPa [31]. The decrease of the CN is interpreted as the fracture of the framework. According to our calculations, the fracture begins beyond 10 GPa.

Previously, it has been reported that the PIA transition of zeolites [40] and ZIFs [29] may be reversible. In order to uncover whether the phase transitions observed in this study are reversible, we release the applied pressure on the framework from following pressures: (i) 2.5 GPa at which the structure remains crystal, (ii) 3.5 GPa at which transition ends, (iii) 10 GPa at which first bond breaking is observed. The total PDFs for these structures are shown in Fig. 2b. Firstly, once the pressure is released from 2.5 GPa, the framework recovers almost the entire volume, but the obtained structure, hereafter referred as ZIF-8-HP, differs slightly from ZIF-8. As previously reported, the imidazolate ligands under pressure freely rotate to increase the accessible pore window. This phenomenon is named "swing effect" and defined by φ angle [41,42] (Fig. S9). The calculated φ angles for ZIF-8 and ZIF-8-HP are 19.8° and 10.6° respectively. These results indicate that ZIF-8 is in a "gate-closed" configuration, and ZIF-8-HP is in a relatively "gate--opened" configuration. Further, the symmetry analysis with KPLOT [43] confirmed that ZIF-8-HP has the same space group symmetry (I43 m) with ZIF-8. Secondly, when the pressure is released from 3.5 GPa the structure recovers approximately 25% its starting volume. Fig. 2b illustrates, beyond the (SRO) there is no significant peak, meaning that framework remains amorphous, referred as a_pZIF-8. Finally, the structure released from 10 GPa recovers 13% of the starting volume, and as expected this structure does not have a long-range order as well.

Fig. 3a shows partial pair distribution functions (PPDF) for ZIF-8, a_pZIF-8 and the experimentally ball-mill amorphized framework, referred as a_mZIF-8. Evidently, $g_{Zn\text{-}N}(r)$ peaks (at 2 and 4 Å) ascribing the bonds between metal and ligand in the crystal structure are preserved in the amorphous structure. Similarly, the C-C (1.3 and 2.1 Å), C-N (1.3, 2.2, 2.6 Å) and N-N (2.2 and 3.2 Å) correlations are retained below 6 Å. The calculated PDFs are well match with experimental data obtained for the ball-mill amorphized ZIF-8 [21], further confirming the validity of our calculations.

To examine the effects of phase transitions on bond angles, we study the key bond angle distributions for ZIF-8 and *a*pZIF-8 (Fig. 3b). In ZIF-8, the N-Zn-N bond angles ($\theta_{N\text{-}Zn\text{-}N}$) are at 108° and 109° depending on whether the bonding is within 4 MR or 6 MR pore windows. On the other hand, the $\theta_{N\text{-}Zn\text{-}N}$ shows a wide range of distribution from 90° to 150° in a_pZIF-8, suggesting that distortions in the tetrahedral units are very effective on the phase transition, or *vice versa*. The Zn-N-C bond angles ($\theta_{Zn\text{-}N\text{-}C}$) are at 122° and 126° in ZIF-8, but it shows a wide distribution from 110° to 135° for the amorphous phase.

To see how the structure behaves in the tensile regime we apply tensile stresses to ZIF-8. The framework's volume linearly increases up to −2.75 GPa and beyond this pressure, the structural failure, which is defined as a tremendous increase in the volume and the breakage of almost all bonds, is observed.

According to the previous reports, ZIF-8 shows a structural anisotropy [31,39]. Therefore, the mechanical properties of the framework are highly dependent on the orientation of applied stresses. In order investigate the effect of direction of uniaxial stresses on the crystal-amorphous phase transition, we apply uniaxial pressure on the framework. The change of the ZIF-8-unit cell volume under uniaxial pressures is shown in Fig. 4. It is obvious that the deformation process occurs in three steps: (i) a linear volumetric reduction of 15% is observed over the pressure range of 0–1.5 GPa; (ii) the framework resists further compression and just small reduction of 7% in the volume occurs up to 4 GPa; (iii) the volume drastically drops between 4 and 5.5 GPa, and the final reduction in the volume is about 50% at 5.5 GPa. Then, the framework partially retrieves to 62% of its starting volume upon the release of pressure. Similar to hydrostatic pressure, the CN of Zn-atoms maintains through all uniaxial pressures. There is no significant difference between uniaxial amorphous phases in terms of density. However, the amorphous phases formed under uniaxial pressure are about 20% denser than the one formed under the hydrostatic pressure (Table S1). The trend in uniaxial P-V curves is in good agreement with Suslick's in situ TEM compression results [31] (Fig. S11). However, critical pressures are overestimated in this work due to the simulation conditions, such as lack of surface effects, fast loading etc.

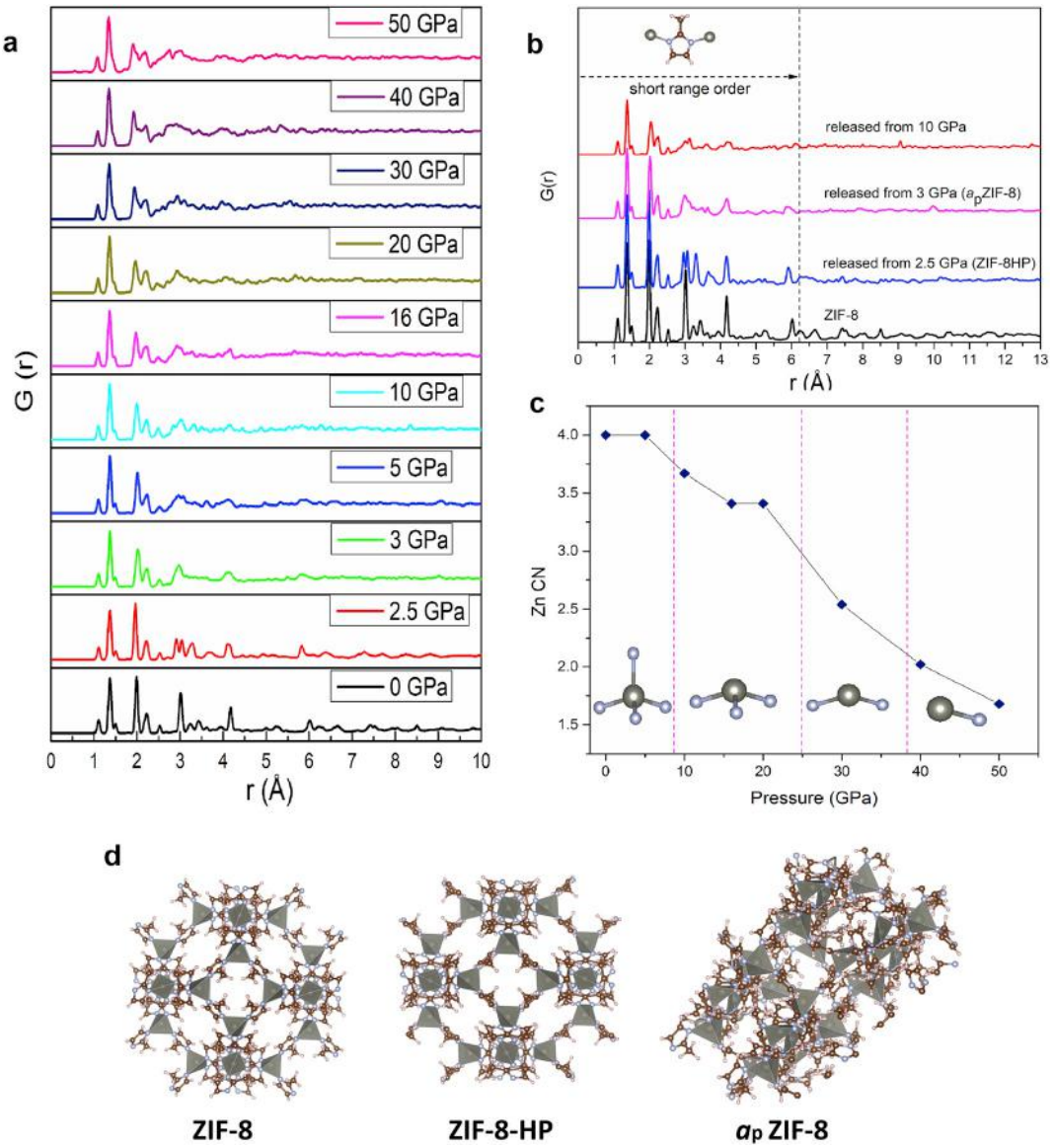

Fig. 2. (a) Total pair distribution functions (PDFs) data for structures formed at 0–50 GP pressure range. (b) Total PDFs for released pressure structures. (c) Coordination number (CN) of Zn as a function of pressure. (d) structural views of the frameworks obtained in this work.

3.2. Mechanical properties

Zero Kelvin elastic constants can be estimated from the energy variation by applying small strains to the equilibrium structure [44,45]. The elastic energy of a solid is defined by

$$E = E_0 + \frac{V}{2}\sum_{i=1}^{6}\sum_{j=1}^{6} C_{ij}e_i e_j + O\left(e_i^3\right) \quad (1)$$

where E_0 and V is the equilibrium energy and volume, respectively, C_{ij} is the elastic constants, e_i and e_j are strains vectors. Due to the symmetry, there are three independent elastic constants C_{11}, C_{12} and C_{44} for a cubic structure. When a volume preserving orthorhombic strain is applied on the lattice:

$$\begin{pmatrix} \delta & 0 & 0 \\ 0 & -\delta & 0 \\ 0 & 0 & \delta^2/\left(1-\delta^2\right) \end{pmatrix}$$

Equation (1) reduces to:

$$E(\delta) = E(0) + (C_{11} - C_{12})V\delta^2 + O\left(\delta^4\right) \quad (2)$$

Additionally, there is a relationship between bulk modulus and those two elastic constants,

$$K = \frac{1}{3}(C_{11} + 2C_{12}) \quad (3)$$

To calculate C_{44}, a volume preserving monoclinic strain is applied,

$$\begin{pmatrix} 0 & \delta & 0 \\ \delta & 0 & 0 \\ 0 & 0 & \delta^2/\left(1-\delta^2\right) \end{pmatrix}$$

In this case, Equation (1) transform into:

$$E(\delta) = E(0) + 2C_{44}V\delta^2 + O\left(\delta^4\right) \quad (4)$$

After for each set of strain calculation, data were fitted to (2) and (4) equations to obtain C_{11}, C_{12} and C_{44} [45]. Also, it is possible to calculate the useful elastic properties for polycrystals by Voigt, Reuss and Hill approximations with elastic constants of single crystals [46]. According to these approximations, shear modulus G is defined by,

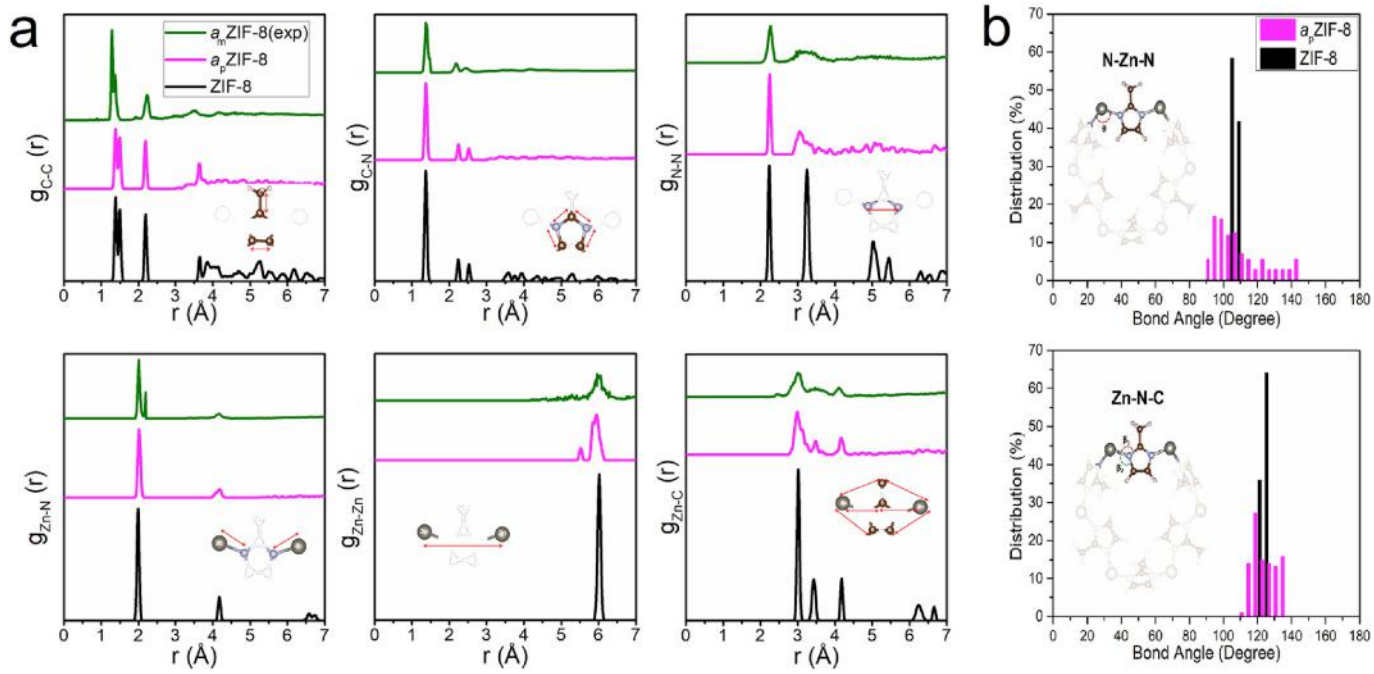

Fig. 3. (a) Partial pair distribution functions of ZIF-8, ZIF-8-HP and a_pZIF-8, and a_mZIF-8. (b) Bond angle distributions for ZIF-8 and a_pZIF-8.

$$5G_{Voigt} = C_{11} - C_{12} + 3C_{44}$$
$$\frac{5}{G_{Reuss}} = 4(S_{11} - S_{12}) + 3S_{44} \quad (5)$$
$$G_{Hill} = \frac{1}{2}\left(G_{Reuss} + G_{Voigt}\right)$$

where S_{ij} are elements of elastic compliance matrix (S), which is inverse of elastic constants matrix. Moreover, Young's modulus (E), Poisson's ratio (ν), and the sound wave velocities; transverse (v_t), longitudinal (v_l) and mean (v_m) are derived by using G_H (shear modulus by Hill approximation), E, ν and K_H (bulk modulus by Hill approximation) (Equation (6)) [46].

$$E = \frac{9K_H}{\left(1 + \frac{3K_H}{G_H}\right)}$$

$$\nu = \frac{\frac{1}{2}\left(K_H - \frac{2}{3}G_H\right)}{\left(K_H + \frac{1}{3}G_H\right)} \quad (6)$$

$$v_t = \sqrt{\frac{G_H}{\rho}},\ v_t = \left(\frac{E(1-\nu)}{\rho(1+\nu)(1-2\nu)}\right),\ v_m = \left(\frac{1}{3}\left(\frac{2}{v_t^3} + \frac{1}{v_l^3}\right)\right)^{-1/3}$$

The elastic and mechanical constants of ZIF-8 obtained in this work are shown in Table 1 and comparable with available data in the literature [39,47].

For a more accurate determination of pressure region where the framework is subjected to elastic and plastic deformation, ZIF-8 was exposed to uniaxial pressure between 1.5 and −1.5 GPa,with an increment of ΔP = 0.1 GPa. The stress-strain curves are shown in Fig. 5. As previously reported [39] and it is clearly apparent from calculations *-vide supra-*, the framework shows a slight anisotropy with the highest strength on x-axis. The average Young's modulus, E_{avg}, obtained from the slope of the stress-strain curve in elastic region is 5.6 GPa, which is consistent with the experimental value. (E_{load} = 4.6 GPa) [31]. The most important result to be noted here is that the compression and tensile strength of the material are very different from each other. Accordingly, the tensile strength of the structure is 50% higher than its compression strength. While ductile materials generally have the same compression and tension strengths, they can be different for brittle materials [48]. Such a distinct behavior has been also observed in lamellar and porous bones [48]. Analogous to compact bones, ZIF-8 is mechanically weak against to compression forces since the structure is highly porous. Still, due to the flexible nature of the framework it shows relatively higher tensile strength.

Poisson's ratio of ZIF-8 was calculated from the strain values obtained in this regime, with following formula:

$$\nu_{ij} = -\frac{\Delta L_i / L_i}{\Delta L_j / L_j} \quad (7)$$

where L_{ij} are the diagonal terms of the lattice parameters. For compression and tension regions, six different Poisson's ratios were estimated. The averaged Poisson's ratio obtained for the applied compression and tension stresses are 0.4 and 0.5, respectively. The compression value is well match with both Poisson's ratios in the literature [39] and predicted using the Hill approximation in this work.

To summarize and compare, the elastic moduli of metals and metal alloys are around 100 GPa and above, and their Poisson's ratios are in the range of 0.2–0.3. Ceramics have relatively lower elastic modulus (typically E~60–70 GPa), and Poisson's ratio (v~0.2). Polymers have very low elastic modulus (E~1–3.5 GPa) and very high Poisson's ratios (0.4–05). As confirmed by our results and other studies [49] in the literature, ZIF-8 is mechanically very similar to polymeric materials (Table S2).

3.3. Electronic properties

The calculated partial density of states (PDOS) and total density of states (TDOS) for ZIF-8 and a_pZIF-8 are shown in Fig. 6a and b, respectively. Both phases demonstrate similar features in the DOS curves. The energy bands between −18 and −10 eV mainly consist of 1s electronic state of H and 2s electronic states of N and C atoms. More significantly, in the upper portion of valence band (VB), where from −7.5 eV to −2.5 eV, a hybridization occurs between 1s-state of H, 2s-,

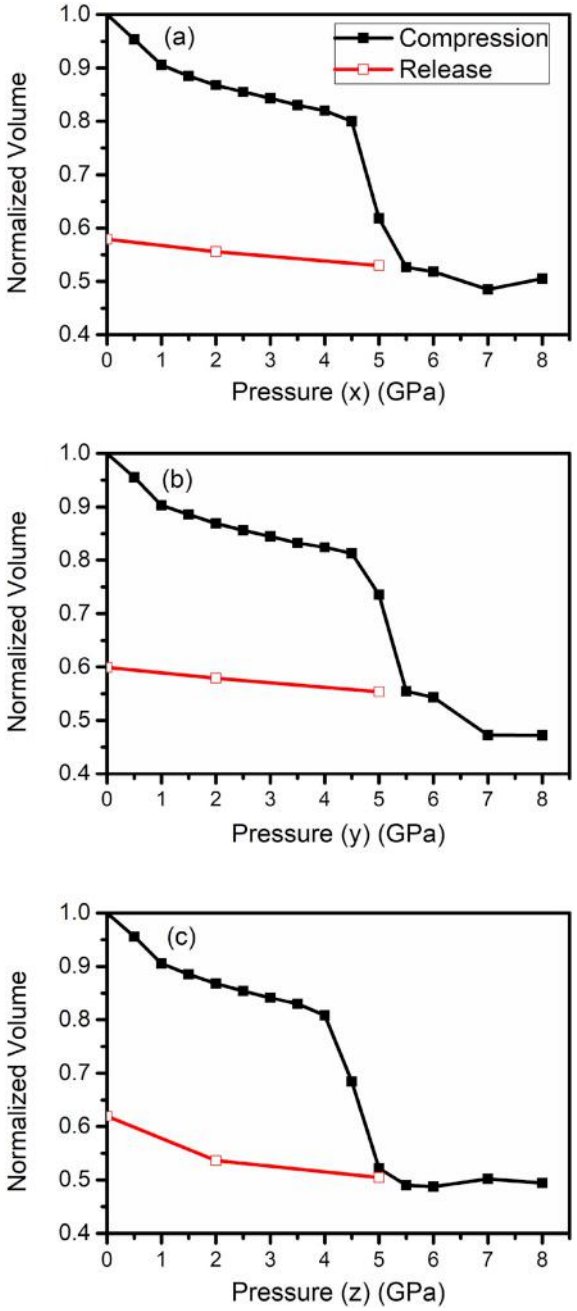

Fig. 4. The uniaxial pressure dependence of ZIF-8 unit cell.

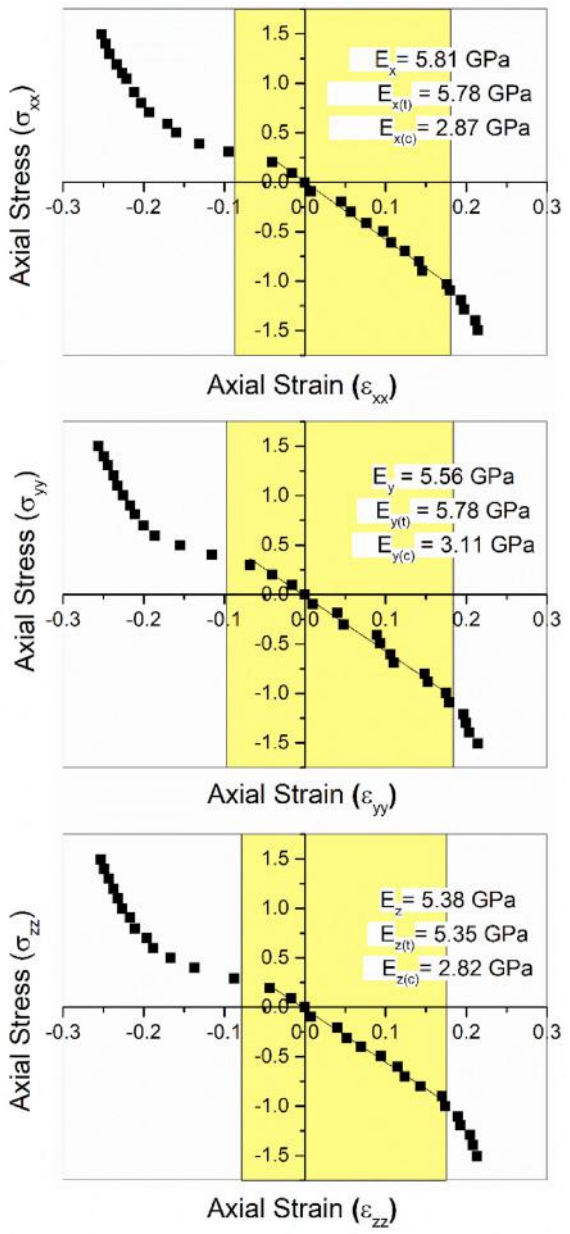

Fig. 5. Stress-strain curves of ZIF-8 unit cell.

2p-states of N and C and 3d state of Zn, indicating the covalent bonds on imidazole ring and coordination bond between Zn and N. In contrast to discontinuous structure of VB, the conduction band (CB) has a continuous form. The sharp peak in CB is assigned to hybridization of 2p-states of N and C atoms. The most likely underestimated band gap for ZIF-8 and a_pZIF-8 due to the ground state formalism of DFT is 4.4 and 4.3 eV, respectively. These results indicate that ZIF-8 and a_pZIF-8 are good insulator. Clearly, a crystal-amorphous phase transition in ZIF-8 does not significantly alter the electronic properties of the framework, despite the changes in charge distributions, bond lengths and bond angles. The most important reason of such an observation is that the electronic structure of ZIF-8 is dominated by insulating 2-methylimidazole ligands [50]. For example, as reported in our previous study [51], the band gap of MOF-5, which is containing relatively conductive terephthalic acid (BDC), significantly decreases under a crystal-amorphous phase transition.

4. Conclusions

We have presented the pressure-induced amorphization of ZIF-8, and its mechanical and electronic properties by using ab initio molecular dynamics simulations. The Parinello-Rahman algorithm appears to be very successful in reproducing experimentally observed crystal-crystal and crystal-amorphous phase transitions. The overestimated critical pressures can be ascribed to the simulation conditions, such as lack of surface effects due to the periodic boundary conditions, non-defective structure etc. All mechanical properties of ZIF-8 are accurately estimated by using two different approaches, and interestingly like compact bones, different compression and tensile strengths are proposed for the crystalline framework. The electronic properties of ZIFs are mostly governed by imidazolate linkers. Since the imidazolate retains its structural integrity, the crystal-amorphous phase transformation does not have significant impact on the electronic properties of ZIF-8. Results are expected to enhance understanding of structural evaluations of ZIFs under different pressure. Pressure-induced amorphization of various

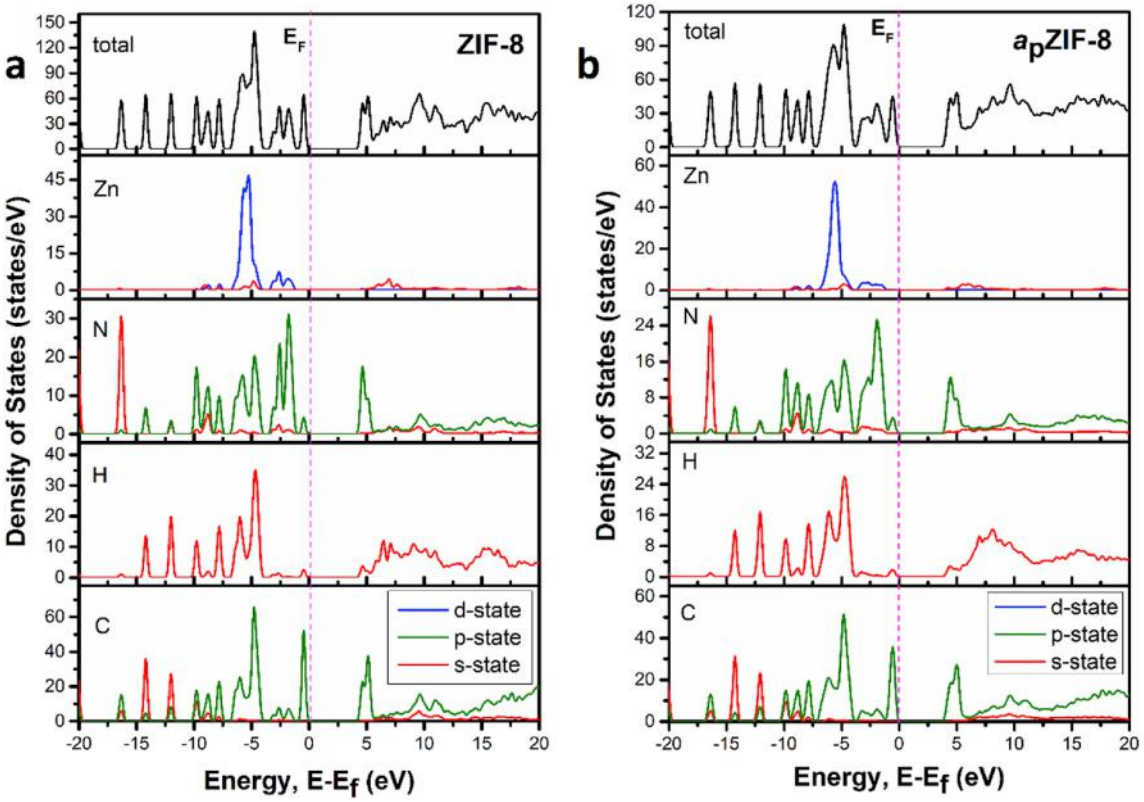

Fig. 6. Calculated total and partial density of states (DOS) for (a) ZIF-8 and (b) a_pZIF-8.

ZIFs and MOFs are also under investigation by the authors.

Conflict of interest statement

The authors declare no competing financial interest.

Acknowledgements

We would like to thank Dr. T. D. Bennett for sharing the experimental data with us. This work was supported by Abdullah Gül University Scientific Research Projects (BAP) under contract number FBA-2017-86. M.E. thanks to (TÜBİTAK). "2214-A International Research Fellowship Program for PhD Students with the grant number 1059B141700539" for his scholarship. The calculations were run on The Scientific and Technological Research Council of Turkey (TÜBİTAK) ULAKBILIM, High Performance and Grid Computing Center (TRUBA) resources.

Appendix A. Supplementary data

Supplementary data to this article can be found online at https://doi.org/10.1016/j.matchemphys.2019.122222.

References

[1] S.M. Sharma, S.K. Sikka, Pressure induced amorphization of materials, Prog. Mater. Sci. 40 (1996) 1–77.
[2] D. Machon, F. Meersman, M.C. Wilding, M. Wilson, P.F. McMillan, Pressure-induced amorphization and polyamorphism: inorganic and biochemical systems, Prog. Mater. Sci. 61 (2014) 216–282.
[3] O. Mishima, L.D. Calvert, E. Whalley, Melting ice-I at 77-K and 10-kbar - a new method of making amorphous solids, Nature 310 (1984) 393–395.
[4] K.J. Kingma, R.J. Hemley, H.K. Mao, D.R. Veblen, New high-pressure transformation in alpha-quartz, Phys. Rev. Lett. 70 (1993) 3927–3930.
[5] S.K. Deb, M. Wilding, M. Somayazulu, P.F. McMillan, Pressure-induced amorphization and an amorphous-amorphous transition in densified porous silicon, Nature 414 (2001) 528–530.
[6] S.M.J. Rogge, M. Waroquier, V. Van Speybroeck, Reliably modeling the mechanical stability of rigid and flexible metal-organic frameworks, Accounts Chem. Res. 51 (2018) 138–148.
[7] J.Z. Zhang, Y.S. Zhao, H.W. Xu, M.V. Zelinskas, L.P. Wang, Y.B. Wang, T. Uchida, Pressure-induced amorphization and phase transformations in beta-LiAlSiO4, Chem. Mater. 17 (2005) 2817–2824.
[8] R.R. Winters, G.C. Serghiou, W.S. Hammack, Observation and explanation of the reversible pressure-induced amorphization of Ca(No3)2/nano3, Phys Rev B 46 (1992) 2792–2797.
[9] K.S. Park, Z. Ni, A.P. Côté, J.Y. Choi, R. Huang, F.J. Uribe-Romo, H.K. Chae, M. O'Keeffe, O.M. Yaghi, Exceptional chemical and thermal stability of zeolitic imidazolate frameworks, Proc. Natl. Acad. Sci. 103 (2006) 10186–10191.
[10] L. Mu, B. Liu, H. Liu, Y.T. Yang, C.Y. Sun, G.J. Chen, A novel method to improve the gas storage capacity of ZIF-8, J. Mater. Chem. 22 (2012) 12246–12252.
[11] D.K. Panchariya, R.K. Rai, E.A. Kumar, S.K. Singh, Core-shell zeolitic imidazolate frameworks for enhanced hydrogen storage, ACS Omega 3 (2018) 167–175.
[12] R. Banerjee, A. Phan, B. Wang, C. Knobler, H. Furukawa, M. O'Keeffe, O.M. Yaghi, High-throughput synthesis of zeolitic imidazolate frameworks and application to CO2 capture, Science 319 (2008) 939–943.
[13] M. Erkartal, U. Erkilic, B. Tam, H. Usta, O. Yazaydin, J.T. Hupp, O.K. Farha, U. Sen, From 2-methylimidazole to 1,2,3-triazole: a topological transformation of ZIF-8 and ZIF-67 by post-synthetic modification, Chem Commun 53 (2017) 2028–2031.
[14] A. Schejn, A. Aboulaich, L. Balan, V. Falk, J. Lalevee, G. Medjahdi, L. Aranda, K. Mozet, R. Schneider, Cu2+-doped zeolitic imidazolate frameworks (ZIF-8): efficient and stable catalysts for cycloadditions and condensation reactions, Catal Sci Technol 5 (2015) 1829–1839.
[15] Y.B. Huang, Y.H. Zhang, X.X. Chen, D.S. Wu, Z.G. Yi, R. Cao, Bimetallic alloy nanocrystals encapsulated in ZIF-8 for synergistic catalysis of ethylene oxidative degradation, Chem Commun 50 (2014) 10115–10117.
[16] C.L. Whitford, C.J. Stephenson, D.A. Gomez-Gualdron, J.T. Hupp, O.K. Farha, R. Q. Snurr, P.C. Stair, Elucidating the nanoparticle metal organic framework interface of Pt@ZIF-8 catalysts, J. Phys. Chem. C 121 (2017) 25079–25091.
[17] W.J. Ma, Q. Jiang, P. Yu, L.F. Yang, L.Q. Mao, Zeolitic imidazolate framework-based electrochemical biosensor for in vivo electrochemical measurements, Anal. Chem. 85 (2013) 7550–7557.
[18] Y.L. Wang, P.F. Hou, Z. Wang, P. Kang, Zinc imidazolate metal-organic frameworks (ZIF-8) for electrochemical reduction of CO2 to CO, ChemPhysChem 18 (2017) 3142–3147.
[19] M. Erkartal, H. Usta, M. Citir, U. Sen, Proton conducting poly(vinyl alcohol) (PVA)/poly (2-acrylamido-2-methylpropane sulfonic acid) (PAMPS)/zeolitic imidazolate framework (ZIF) ternary composite membrane, J. Membr. Sci. 499 (2016) 156–163.
[20] K.S. Park, Z. Ni, A.P. Cote, J.Y. Choi, R.D. Huang, F.J. Uribe-Romo, H.K. Chae, M. O'Keeffe, O.M. Yaghi, Exceptional chemical and thermal stability of zeolitic imidazolate frameworks, P Natl Acad Sci USA 103 (2006) 10186–10191.

[21] S. Cao, T.D. Bennett, D.A. Keen, A.L. Goodwin, A.K. Cheetham, Amorphization of the prototypical zeolitic imidazolate framework ZIF-8 by ball-milling, Chem Commun 48 (2012) 7805–7807.
[22] K.W. Chapman, G.J. Halder, P.J. Chupas, Pressure-induced amorphization and porosity modification in a metal-organic framework, J. Am. Chem. Soc. 131 (2009) 17546–17547.
[23] S.C. McKellar, S.A. Moggach, Structural studies of metal-organic frameworks under high pressure, Acta Crystallogr. B 71 (2015) 587–607.
[24] T.D. Bennett, A.K. Cheetham, Amorphous metal-organic frameworks, Accounts Chem. Res. 47 (2014) 1555–1562.
[25] S. Tanaka, K. Fujita, Y. Miyake, M. Miyamoto, Y. Hasegawa, T. Makino, S. Van der Perre, J.C. Saint Remi, T. Van Assche, G.V. Baron, J.F.M. Denayer, Adsorption and diffusion phenomena in crystal size engineered ZIF-8 MOF, J. Phys. Chem. C 119 (2015) 28430–28439.
[26] C.L. Hobday, C.H. Woodall, M.J. Lennox, M. Frost, K. Kamenev, T. Duren, C. A. Morrison, S.A. Moggach, Understanding the adsorption process in ZIF-8 using high pressure crystallography and computational modelling, Nat. Commun. 9 (2018).
[27] H. Tanaka, S. Ohsaki, S. Hiraide, D. Yamamoto, S. Watanabe, M.T. Miyahara, Adsorption-induced structural transition of ZIF-8: a combined experimental and simulation study, J. Phys. Chem. C 118 (2014) 8445–8454.
[28] F.X. Coudert, Molecular mechanism of swing effect in zeolitic imidazolate framework ZIF-8: continuous deformation upon adsorption, ChemPhysChem 18 (2017) 2732–2738.
[29] T.D. Bennett, P. Simoncic, S.A. Moggach, F. Gozzo, P. Macchi, D.A. Keen, J.C. Tan, A.K. Cheetham, Reversible pressure-induced amorphization of a zeolitic imidazolate framework (ZIF-4), Chem Commun 47 (2011) 7983–7985.
[30] Y. Hu, H. Kazemian, S. Rohani, Y.N. Huang, Y. Song, In situ high pressure study of ZIF-8 by FTIR spectroscopy, Chem Commun 47 (2011) 12694–12696.
[31] Z. Su, Y.R. Miao, S.M. Mao, G.H. Zhang, S. Dillon, J.T. Miller, K.S. Suslick, Compression-induced deformation of individual metal-organic framework microcrystals, J. Am. Chem. Soc. 137 (2015) 1750–1753.
[32] J.M. Soler, E. Artacho, J.D. Gale, A. Garcia, J. Junquera, P. Ordejon, D. Sanchez-Portal, The SIESTA method for ab initio order-N materials simulation, J Phys-Condens Mat 14 (2002) 2745–2779.
[33] J.P. Perdew, K. Burke, M. Ernzerhof, Generalized gradient approximation made simple, Phys. Rev. Lett. 77 (1996) 3865–3868.
[34] N. Troullier, J.L. Martins, Efficient pseudopotentials for plane-wave calculations, Phys Rev B 43 (1991) 1993–2006.
[35] M. Parrinello, A. Rahman, Polymorphic transitions in single-crystals - a new molecular-dynamics method, J. Appl. Phys. 52 (1981) 7182–7190.
[36] A.J. Graham, D.R. Allan, A. Muszkiewicz, C.A. Morrison, S.A. Moggach, The effect of high pressure on MOF-5: guest-induced modification of pore size and content at high pressure, Angew. Chem. Int. Ed. 50 (2011) 11138–11141.
[37] K. Momma, F. Izumi, VESTA 3 for three-dimensional visualization of crystal, volumetric and morphology data, J. Appl. Crystallogr. 44 (2011) 1272–1276.
[38] S. Le Roux, V. Petkov, ISAACS - interactive structure analysis of amorphous and crystalline systems, J. Appl. Crystallogr. 43 (2010) 181–185.
[39] J.C. Tan, B. Civalleri, C.C. Lin, L. Valenzano, R. Galvelis, P.F. Chen, T.D. Bennett, C. Mellot-Draznieks, C.M. Zicovich-Wilson, A.K. Cheetham, Exceptionally low shear modulus in a prototypical imidazole-based metal-organic framework, Phys. Rev. Lett. 108 (2012).
[40] I. Peral, J. Iniguez, Amorphization induced by pressure: results for zeolites and general implications, Phys. Rev. Lett. 97 (2006).
[41] W. Zhang, J. Maul, D. Vulpe, P.Z. Moghadam, D. Fairen-Jimenez, D.M. Mittleman, J.A. Zeitler, A. Erba, M.T. Ruggiero, Probing the mechanochemistry of metal-organic frameworks with low-frequency vibrational spectroscopy, J. Phys. Chem. C 122 (2018) 27442–27450.
[42] J. Maul, M.R. Ryder, M.T. Ruggiero, A. Erba, Pressure-driven mechanical anisotropy and destabilization in zeolitic imidazolate frameworks, Phys Rev B 99 (2019).
[43] R. Hundt, J.C. Schon, A. Hannemann, M. Jansen, Determination of symmetries and idealized cell parameters for simulated structures, J. Appl. Crystallogr. 32 (1999) 413–416.
[44] P. Ravindran, L. Fast, P.A. Korzhavyi, B. Johansson, J. Wills, O. Eriksson, Density functional theory for calculation of elastic properties of orthorhombic crystals: application to TiSi2, J. Appl. Phys. 84 (1998) 4891–4904.
[45] S.Q. Wang, H.Q. Ye, Ab initio elastic constants for the lonsdaleite phases of C, Si and Ge, J Phys-Condens Mat 15 (2003) 5307–5314.
[46] C.A. Ponce, R.A. Casali, M.A. Caravaca, Ab initio study of mechanical and thermo-acoustic properties of tough ceramics: applications to HfO2 in its cubic and orthorhombic phase, J Phys-Condens Mat 20 (2008).
[47] A.U. Ortiz, A. Boutin, A.H. Fuchs, F.X. Coudert, Investigating the pressure-induced amorphization of zeolitic imidazolate framework ZIF-8: mechanical instability due to shear mode softening, J. Phys. Chem. Lett. 4 (2013) 1861–1865.
[48] M.M. Barak, J.D. Currey, S. Weiner, R. Shahar, Are tensile and compressive Young's moduli of compact bone different? J Mech Behav Biomed 2 (2009) 51–60.
[49] J.C. Tan, T.D. Bennett, A.K. Cheetham, Chemical structure, network topology, and porosity effects on the mechanical properties of Zeolitic Imidazolate Frameworks, P Natl Acad Sci USA 107 (2010) 9938–9943.
[50] K.T. Butler, S.D. Worrall, C.D. Molloy, C.H. Hendon, M.P. Attfield, R.A.W. Dryfe, A. Walsh, Electronic structure design for nanoporous, electrically conductive zeolitic imidazolate frameworks, J. Mater. Chem. C 5 (2017) 7726–7731.
[51] M. Erkartal, M. Durandurdu, Pressure-induced amorphization of MOF-5: a first principles study, Chemistry 3 (2018) 8056–8063.